

DEPARTMENT OF THE ARMY  
U.S. Army Corps of Engineers  
Washington, DC 20314-1000

CECW-ED

ETL 1110-2-344

Technical Letter  
No. 1110-2-344

31 December 1993

Engineering and Design  
FRACTURE MECHANICS ANALYSIS OF A  
GRAVITY LOCK MONOLITH

## **Distribution Restriction Statement**

Approved for public release; distribution is unlimited.

**Engineering and Design  
FRACTURE MECHANICS ANALYSIS OF A  
GRAVITY LOCK MONOLITH****1. Purpose**

This engineer technical letter (ETL) provides supplemental guidance on applying the principles of finite element analysis coupled with fracture mechanics to assess the safety and serviceability of existing concrete hydraulic structures (CHS). This guidance is intended to supplement that guidance provided in ETL 1110-8-16(FR).

**2. Applicability**

This ETL applies to HQUSACE elements, major subordinate commands, districts, laboratories, and field operating activities having responsibilities for the design of civil works projects.

**3. References**

- a. ETL 1110-2-22, Design of Navigation Lock Gravity Walls.
- b. ETL 1110-2-310, Stability Criteria for Existing Concrete Navigation Structures on Rock Foundations.
- c. ETL 1110-8-16(FR). Fracture Mechanics Analysis of Concrete Hydraulic Structures.
- d. Reich, R. W. 1992. *On the Marriage of Mixed Finite Element Methods and Fracture Mechanics: An Application to Concrete Dams*, Ph.D Thesis, University of Colorado, Boulder.
- e. Reich, R. W., Cervenka, J., and Saouma, V. E. 1991. *Merlin User's Manual*, University of Colorado, Boulder.

f. Stern, M., Becker, E. B., and Dunham, R. S. 1976. "A Contour Integral Computation of Mixed-Mode Stress Intensity Factors," *International Journal of Fracture*, Vol. 12, No. 3, pp. 359-368.

g. Zienkiewicz, O. C., Violette, J. P., Toyoshima, S., and Nakazawa, S. 1985. "Iterative Method for Constrained and Mixed Approximations. An Inexpensive Improvement of FEM Performance," *Computer Methods in Applied Mechanics and Engineering*, Vol. 51, Nos. 1-3, pp. 3-29.

**4. Background**

a. *Previous design practice.* Previous design practice for evaluating structural stability of CHS has been based on a static, rigid body equilibrium analysis. ETL 1110-2-22 and ETL 1110-2-310 were published as guidance for conducting such evaluation of existing navigation structures. Numerous safety and rehabilitation evaluations of existing CHS have indicated potential structural distress for project conditions which were not consistent with observations and measurements of satisfactory structural performance.

b. *Current practice.* Advances in modern structural analysis techniques including finite element analysis and fracture mechanics provide a more realistic basis for evaluation of existing CHS. ETL 1110-8-16(FR) was published to provide guidance on applying the principles of fracture mechanics to assess the safety and serviceability of existing CHS. This ETL is intended to provide supplemental guidance on finite element modeling and application of fracture mechanics for CHS. Appendix A provides guidance on modeling of uplift pressures acting at the base of a CHS and an example

including a detailed fracture mechanics based finite element analysis of a gravity lock monolith with a large culvert. Appendix B includes an analysis of the same monolith with the exception that the culvert is excluded. Appendix B is provided to show the effects that a large void such as a culvert may have on the analysis. Appendix C provides an example for the monolith of the example provided in Appendix A with the exception that uplift pressures along the base of the monolith are not included. Appendix C is provided to compare the traditional method of analysis with a simplified fracture mechanics analysis without uplift.

### **5. Objective**

This ETL is the second of a series which will provide guidance on modern techniques for

FOR THE DIRECTOR OF CIVIL WORKS:

- 3 Appendixes
- APP A - Fracture Mechanics Based Analysis of a Gravity Lock Monolith
- APP B - Analyses With No Culvert
- APP C - Analyses With No Uplift

evaluating the stability and strength of existing CHS. This ETL provides supplemental guidance to that included in ETL 1110-8-16(FR) for finite element modeling and structural evaluation for CHS using a fracture mechanics based analysis.

### **6. Action**

The guidance provided in the enclosures should be followed when conducting a fracture mechanics based analysis. A fracture mechanics based analysis should be performed according to the requirements of ETL 1110-8-16(FR).



PAUL D. BARBER, PE  
Chief, Engineering Division  
Directorate of Civil Works

## APPENDIX A: FRACTURE MECHANICS BASED ANALYSIS OF A GRAVITY LOCK MONOLITH

### 1. Introduction

*a. Traditional practice.* Traditional design practice for evaluating structural stability of gravity structures is currently based on an approximate technique (see paragraph 2) which produces conservative results in the prediction of cracking. A fracture mechanics based analysis is an improved method which may be used to predict cracking and to perform a structural evaluation. ETL 1110-8-16(FR) states that a fracture mechanics analysis should be performed if current stability and strength criteria indicate that major structural rehabilitation is necessary because overturning instability and cracking are predicted. In this enclosure, a fracture mechanics based analysis combined with a finite element structural analysis is described. A specific example using fracture mechanics analysis is provided for the evaluation of the strength and stability of a gravity lock monolith at Locks No. 27 on the Mississippi River. Guidance on finite element modeling and the application of fracture mechanics is described in detail.

*b. Locks No. 27, Monolith 7E.* Locks No. 27 are located at mile 185.1 (km 298.01) of the Mississippi River navigation channel. The locks are part of the Chain of Rocks Canal which allows river traffic to bypass the Chain of Rocks low water dam (Dam No. 27). These locks consist of a 1,200-ft-long main lock and a 600-ft-long auxiliary lock, both with 110-ft-wide chambers. The lock walls consist of gravity monoliths founded on rock. The analyses were performed on monolith 7E because traditional analysis indicated that this monolith was the most critical. Monolith 7E is located on the east landwall of the main lock approximately 200 ft downstream from the upstream lock gate. Monolith 7E is 34.5 ft long, and a typical cross section is shown in Figure A-1. The monolith is constructed in a 3-ft deep key as shown in Figure A-1. For the examples described herein, the effect of the key is ignored; and it is assumed that the foundation interface is at elevation 340 ft.

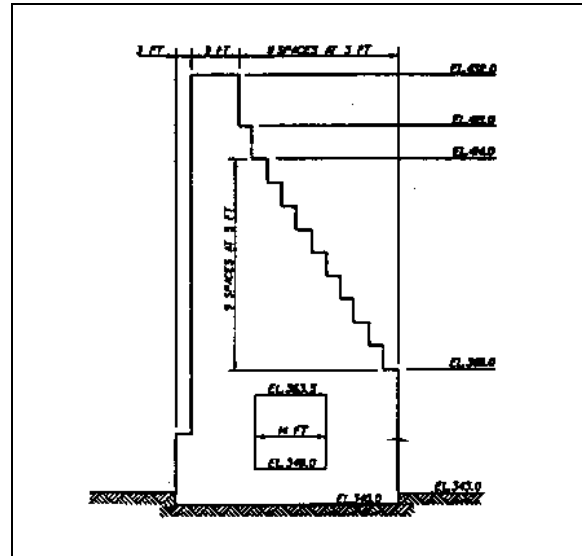


Figure A-1. Locks 27 monolith 7E cross section

### 2. Current Design Practice

*a. Analysis.* Current design practice to determine sliding and overturning stability of concrete navigation structures is to perform a static, rigid body equilibrium analysis (subsequently referred to as the traditional analysis). This analysis is generally performed assuming that no tensile forces can be transferred across the concrete/rock interface at the base of the structure. The effects of uplift, bearing, backfill, backfill saturation, lock chamber water level, and the geometry of the structure should be considered. The static, rigid body equilibrium analysis, coupled with the assumed pressure distributions, is used to find both the base compression area and the soil/rock bearing pressure. For the current study (monolith 7E), typical loads and the assumed uplift and bearing pressure distributions are shown in Figure A-2. Full uplift due to hydrostatic pressure was assumed to act under the tension (cracked) area of the base, and a linear distribution for uplift forces was assumed under the compression area.

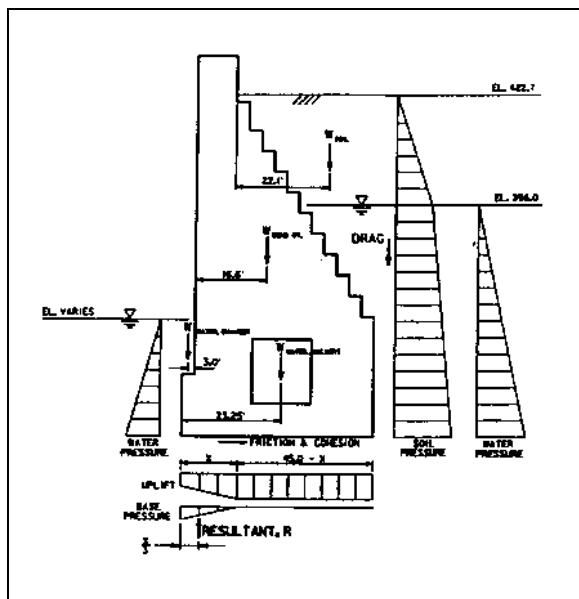


Figure A-2. Critical load combination for monolith 7E

*b. Results.* The classical analysis procedure was performed for a variety of combinations of backfill saturation elevations and lock water elevations (ETL 1110-8-16(FR)). For the current study, results for an actual observed condition with a lock water elevation of 340.0 ft (lock dewatered) and a backfill saturation elevation of 396.0 ft (piezometer reading) are used. Based on these conditions, the traditional analysis results in a calculated percentage of base in compression of 48.6% (51.4% of the base in tension translates to a crack of length 23.13 ft assuming no ability to transmit tensile forces). This does not meet the requirement of at least 75% of base in compression as specified by ETL 1110-2-22 "Design of Navigation Lock Gravity Walls." When the lock was dewatered, no signs of distress were detected, and recent instrumentation has indicated no significant movement of the lock wall.

### 3. Finite Element/Fracture Mechanics Based Analysis

*a. Introduction.* In this section, a fracture mechanics based analysis consisting of a finite element structural analysis supplemented with fracture mechanics is described. A discussion on the modeling of uplift pressures at the base of a gravity structure is included.

#### *b. Uplift pressure models.*

(1) Modeling of uplift pressures at the base of a gravity structure (monolith) requires knowledge of the actual foundation conditions and requires that various assumptions be made as to the magnitude and distribution of pressure. There are many approaches which may be used to model uplift pressures at the base of a gravity structure. Three basic approaches are described by the following cases. In each case the uplift pressure along the cracked portion at the base of the structure is assumed to be constant at a magnitude equal to the hydrostatic pressure at the mouth of the crack.

(a) Case 1. The monolith (concrete) and foundation (rock) are considered impervious and elastic, while the monolith/foundation interface is considered pervious. Uplift pressures are assumed to vary linearly from the crack tip to the toe of the monolith. This corresponds to the pipe flow analogy shown in Figure A-3.

(b) Case 2. The monolith and foundation are considered impervious and elastic. Uplift pressures are computed from piezometer readings taken at several locations along the uncracked portion of the monolith.

(c) Case 3. The monolith is considered impervious and elastic and the foundation is considered impervious and infinitely rigid. Uplift pressures are assumed to vary linearly from the crack tip to the toe of the monolith.

(2) The approach used in this study (described in paragraph 3c) corresponds to Case 1; the same modeling techniques would also be valid for Case 2. Case 3 corresponds to the approach most commonly assumed with the traditional method of analysis.

(3) Using the uplift models defined by Cases 1 and 2 within the context of a finite element analysis requires special considerations. Pressures acting along the interface between the monolith and foundation result in hydrostatic forces of equal magnitude in all directions. In a finite element analysis, if uplift pressures along the uncracked portion of the base are applied to the elements adjacent to the interface between the monolith and the foundation as vertical pressures in equal and opposite

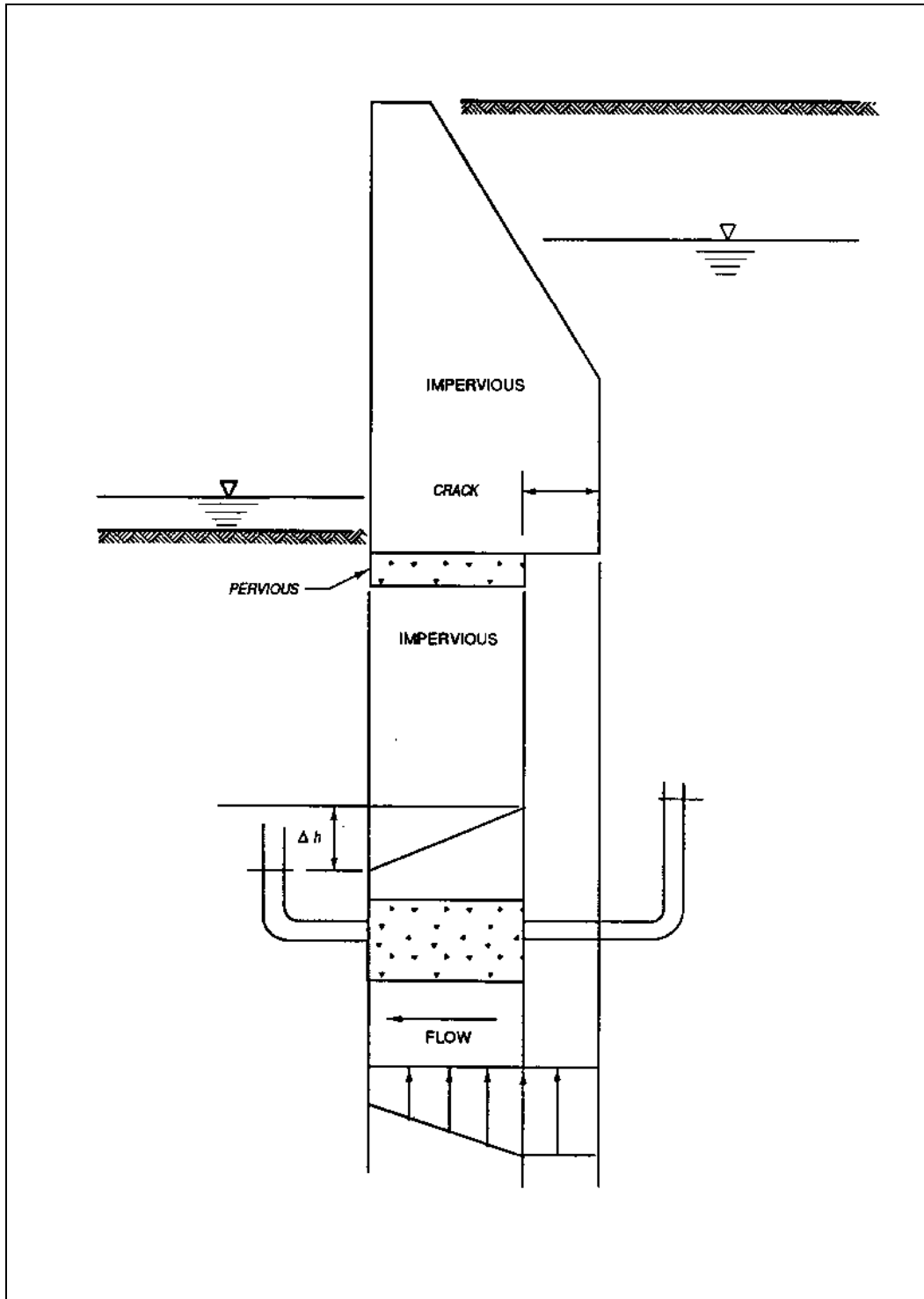


Figure A-3. Pipe flow analogy

directions, the resulting nodal forces cancel. In order to keep the nodal forces due to uplift pressures from canceling, a thin pervious elastic region is placed between the two impervious regions (monolith and foundation). The pervious elastic region simulates the pipe in the pipe flow analogy shown in Figure A-3. This region corresponds to the elements where pore pressures are prescribed as described in paragraph 3c. The result of this approach is that the nodal forces due to the uplift pressures are transferred to the monolith and the foundation one row of elements away from the interface. There is also a small horizontal force due to the pore pressure gradient in the horizontal direction transmitted to the monolith and the foundation which results in some shear stresses. This has only a minor influence on the computation of final crack length.

(4) The uplift model described by Case 3 is only practical for the traditional method of analysis. An infinitely rigid foundation would be modeled in a finite element analysis using either pinned supports or a combination of pinned and roller supports located along the base of the monolith. Since the nodes on the uncracked portion of the base of the monolith are fixed in the vertical direction, it is impossible to prescribe pressures on the base of the monolith. The addition of a thin pervious region at the base, described above for Cases 1 and 2, could also be applied for Case 3.

(5) Regardless of how the analysis is performed, be it either the traditional method or finite element analysis, the most fundamental issue to be addressed in the modeling of uplift pressures is the flow regime. Once the flow regime has been established, the determination of the uplift pressures is rather straightforward. In the absence of field data from piezometers, the assumption of a linear variation in pressure, which corresponds to a true steady-state condition, is the most reasonable. When piezometric data are available, the assumption of a linear variation in pressure between adjacent piezometers may be reasonable, provided the resulting uplift pressure profile is relatively smooth. If drains are present and functioning properly, a seepage flow analysis may be required as the assumption of a linear variation in pressure would be unconservative for this situation. In general, determining uplift pressures from a seepage flow analysis should be avoided unless the permeability

of the rock is fairly well known. This is especially true if the permeability is thought to be anisotropic.

*c. Finite element model.*

(1) The monolith, the backfill above the stair-step pattern on the back side of the monolith, and a portion of the foundation near the monolith are idealized by the finite element mesh shown in Figure A-4. This mesh consists of 1020 elements and 1236 nodes. A rectangular region of the rock foundation, 192 ft wide and 92 ft in depth, is modeled. The vertical plane on the left side of this region is aligned with the center line of the main lock chamber. The left-most vertical face of the monolith is 52 ft to the right of the main lock chamber center line. The entire mesh of the model consists of 4-node quadrilateral elements which include a selective-reduced integration scheme to improve performance for bending modes (Reich 1992). The plane strain idealization is used to define the stress-strain relations for the entire model. Strain and stress values are computed at the nodes using a variational recovery technique (Zienkiewicz et al. 1985).

(2) The material properties for the concrete, rock, soil, and interface are given in Table A-1, where  $E$  is the modulus of elasticity,  $\nu$  the Poisson's ratio,  $\gamma$  the dry unit weight,  $\gamma_s$  the saturated unit weight,  $\gamma_w$  the unit weight of water,  $K_H$  the horizontal earth pressure coefficient, and  $K_V$  the vertical earth pressure coefficient. Elastic properties for the concrete and rock are assumed to be identical. The loads applied to the mesh correspond to those shown in Figure A-2. A lock water elevation of 340.0 ft and a backfill saturation elevation of 396 ft are assumed. For the prediction of cracking, the crack induced by this force system is confined to the interface between the foundation and the monolith.

(a) Bi-material interface. The modeled region includes bi-material interfaces at the base of the monolith (concrete/rock interface) and at the back of the monolith (concrete/soil interface). Special considerations are required to enable the computation of unique nodal strain and stress values for each of the two materials on a bi-material interface. To enforce continuity, yet maintain the ability to compute unique strain and stress values, master and slave nodes have been utilized. Master and slave

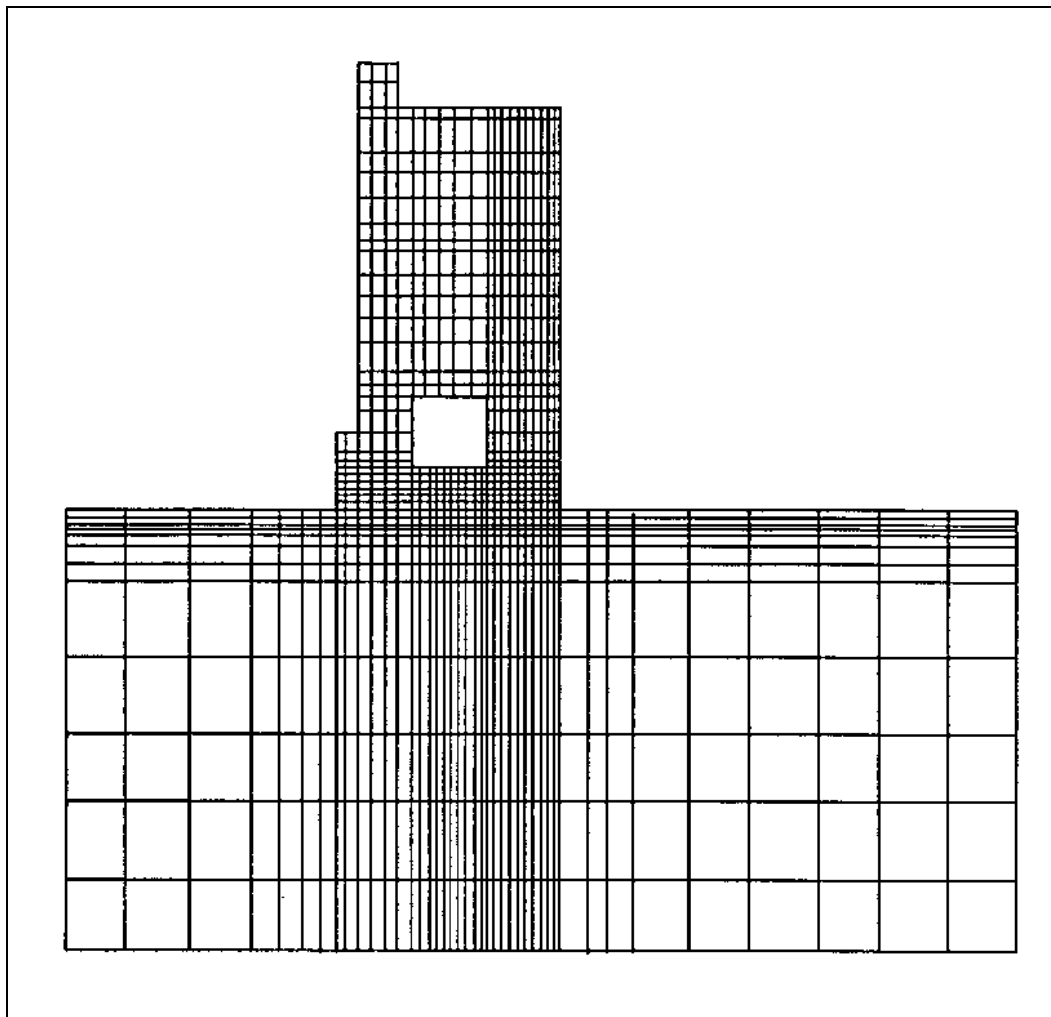


**Figure A-4. Finite element discretization**

nodes are pairs of nodes which occupy the same point in space and are constrained to have identical displacements, but are attached to different elements. Therefore, on bi-material interfaces, displacements of the master and slave nodes are identical; however, unique strain and stress values can be determined.

In the uncracked zone at the base of the monolith, a perfect bond between the rock foundation and the concrete monolith is assumed. The connection between the foundation and the monolith is enforced by defining master and slave nodes along the interface boundary. Cracking on this interface is simulated by eliminating master and slave node constraints, allowing the node pairs to displace independently. On the interface between the backfill and the monolith, a perfect bond is assumed,

even though it might be more appropriate to assume a frictional interface. This assumption was made in an effort to simplify the analyses by eliminating all nonlinear behavior not related to cracking on the interface between the monolith and the foundation. The connection between the backfill and the monolith is enforced through master and slave nodes located on the interface boundary.

(b) Applied forces. The vertical force of the backfill located above the stair-step pattern on the back side of the monolith is applied to the mesh as a body force due to gravity. The vertical force for the backfill above the foundation behind the monolith is applied as a pressure  $p_v$ . The magnitude of  $p_v$  is

$$p_v = H_\gamma + H_s \gamma_s \quad (1)$$

**Table A-1**  
**Material Properties for Locks No. 27**

Concrete	
E	3,500.0 ksi
$\nu$	0.2
$\gamma$	0.150 kip/ft <sup>3</sup>
Rock	
E	3,500.0 ksi
$\nu$	0.2
$\gamma$	0.0 kip/ft <sup>3</sup>
Concrete/Rock Interface	
$K_{ic}$	0.0 ksi $\sqrt{\text{in.}}$
Soil	
E	3.5 ksi
$\nu$	0.35
$\gamma$	0.125 kip/ft <sup>3</sup>
$\gamma_s$	0.130 kip/ft <sup>3</sup>
$\gamma_w$	0.0625 kip/ft <sup>3</sup>
$K_H$	0.45
$K_V$	0.2

where  $H$  is the height of the backfill above the water table and  $H_s$  is the height of the backfill between the water table and the foundation. The vertical (drag) forces due to differential settlement within the backfill acting on the vertical plane defined by the back face of the monolith and passing through the backfill are applied to the mesh as tractions  $t_d$ . The magnitude of  $t_d$  is

$$t_d = K_V K_H \gamma y \quad (2)$$

for  $y \leq H$  and

$$t_d = K_V K_H \gamma H + K_V K_H (\gamma_s - \gamma_w)(y - H) \quad (3)$$

for  $H < y \leq (H + H_s)$ , where  $y$  is the distance below the top of the backfill. The traction  $t_d$  defined in Equation 3 is based on the effective pressure. Figure A-5 illustrates how the pressure  $p_v$  and the traction  $t_d$  are applied to the mesh. The vertical force due to the weight of the monolith is applied as a

gravity body force. There are no gravity body forces applied for the foundation since the deformation due to self weight would have occurred in the foundation before the construction of the lock. Body forces in the foundation are ignored by assigning a value of zero to the unit weight of the rock, as shown in Table A-1. The vertical force for water in the culvert is omitted because the water level in the lock is below the floor of the culvert. Horizontal forces due to hydrostatic and lateral earth pressures acting on the vertical plane defined by the back face of the monolith and passing through the backfill are applied to the mesh as pressures  $p_h$ . The magnitude of  $p_h$  is

$$p_h = K_H \gamma y \quad (4)$$

for  $y \leq H$  and

$$p_h = K_H \gamma H + K_H (\gamma_s - \gamma_w)(y - H) + \gamma_w (y - H) \quad (5)$$

for  $H < y \leq (H + H_s)$ , where  $y$  is the distance below the top of the backfill. Figure A-6 illustrates how the pressure  $p_h$  is applied to the mesh. The horizontal force for water in the lock chamber is not included because the lock is assumed to be dewatered. Uplift pressures are modeled according to Case 1 of paragraph 3b. Uplift pressures at the base of the monolith are applied to the mesh as a combination of pressures and initial stresses. Pressures corresponding to full hydrostatic uplift are applied on the surface of all elements adjacent to the assumed crack surfaces. Initial stresses are applied to the elements which are adjacent to the interface between the monolith and the foundation. The initial stresses  $\sigma_0$  are specified as nodal pore pressures  $p$  and are converted to initial stresses such that

$$\sigma_0 = \begin{Bmatrix} \sigma_{xx_0} \\ \sigma_{yy_0} \\ \sigma_{zz_0} \\ \tau_{xy_0} \end{Bmatrix} = \begin{Bmatrix} -p \\ -p \\ -p \\ 0 \end{Bmatrix} \quad (6)$$

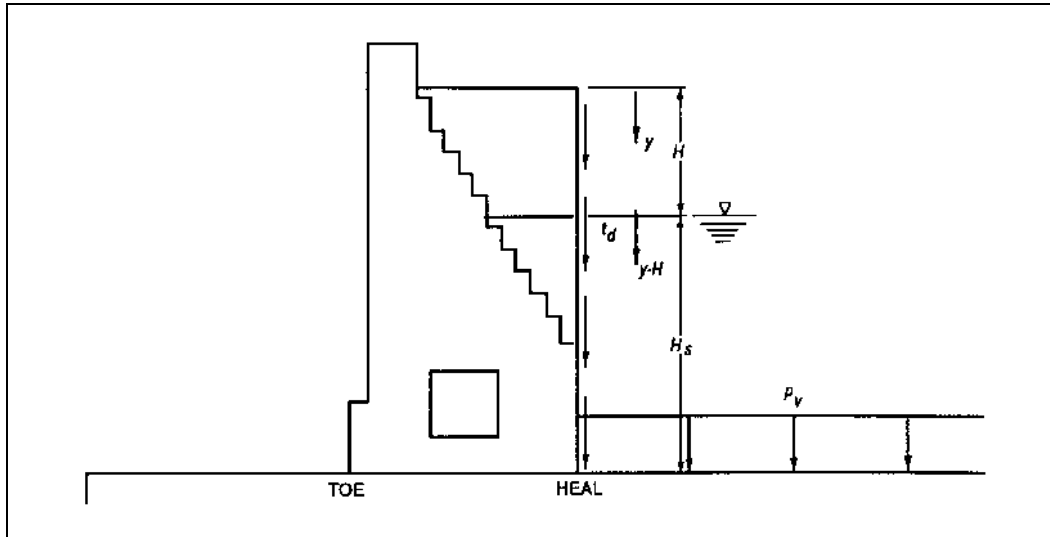


Figure A-5. Pressures from backfill in vertical direction

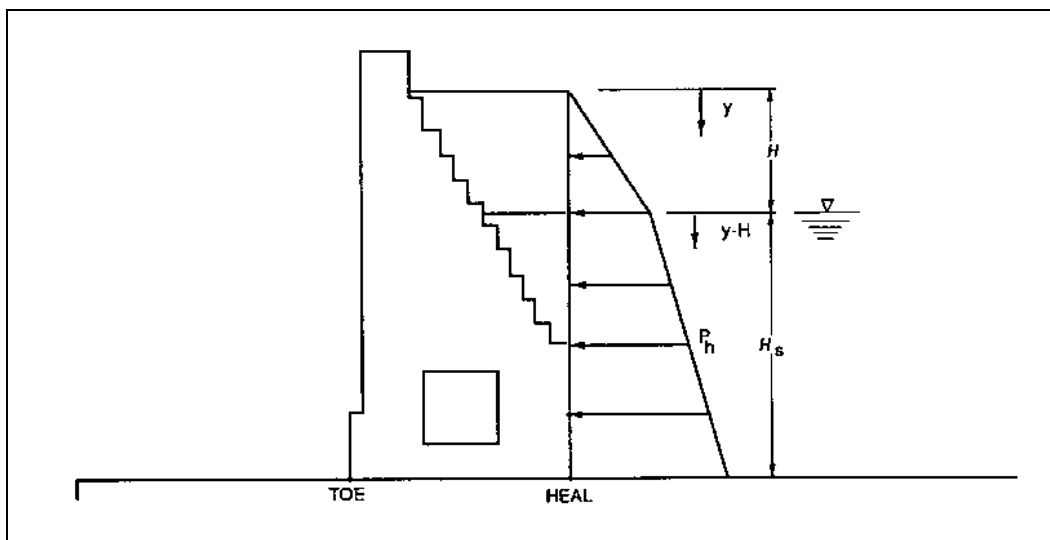


Figure A-6. Pressures from backfill in horizontal direction

for plane strain. The negative sign on the pore pressures  $p$  in Equation 6 reconciles the difference between the sign conventions for soil mechanics and standard solid mechanics. The pore pressures  $p$  correspond to full uplift for those elements adjacent to the crack surfaces and vary linearly in the horizontal direction from full uplift at the crack tip to zero (empty lock chamber) at the toe of the monolith. The initial stresses are constant in the vertical direction at a given horizontal distance from the toe. The pore pressure distribution over the elements adjacent to the interface is shown in Figure A-7.

The equivalent nodal forces  $f_{\sigma_0}$  for the elements subject to the initial stresses are computed as a volume integral over the element domain

$$f_{\sigma_0} = -\int_V B^T \sigma_0 dV \quad (7)$$

where  $B$  is the strain-displacement operator. Because the initial stresses are hydrostatic, the equivalent nodal forces act in both the horizontal and vertical directions. Elements subjected to initial

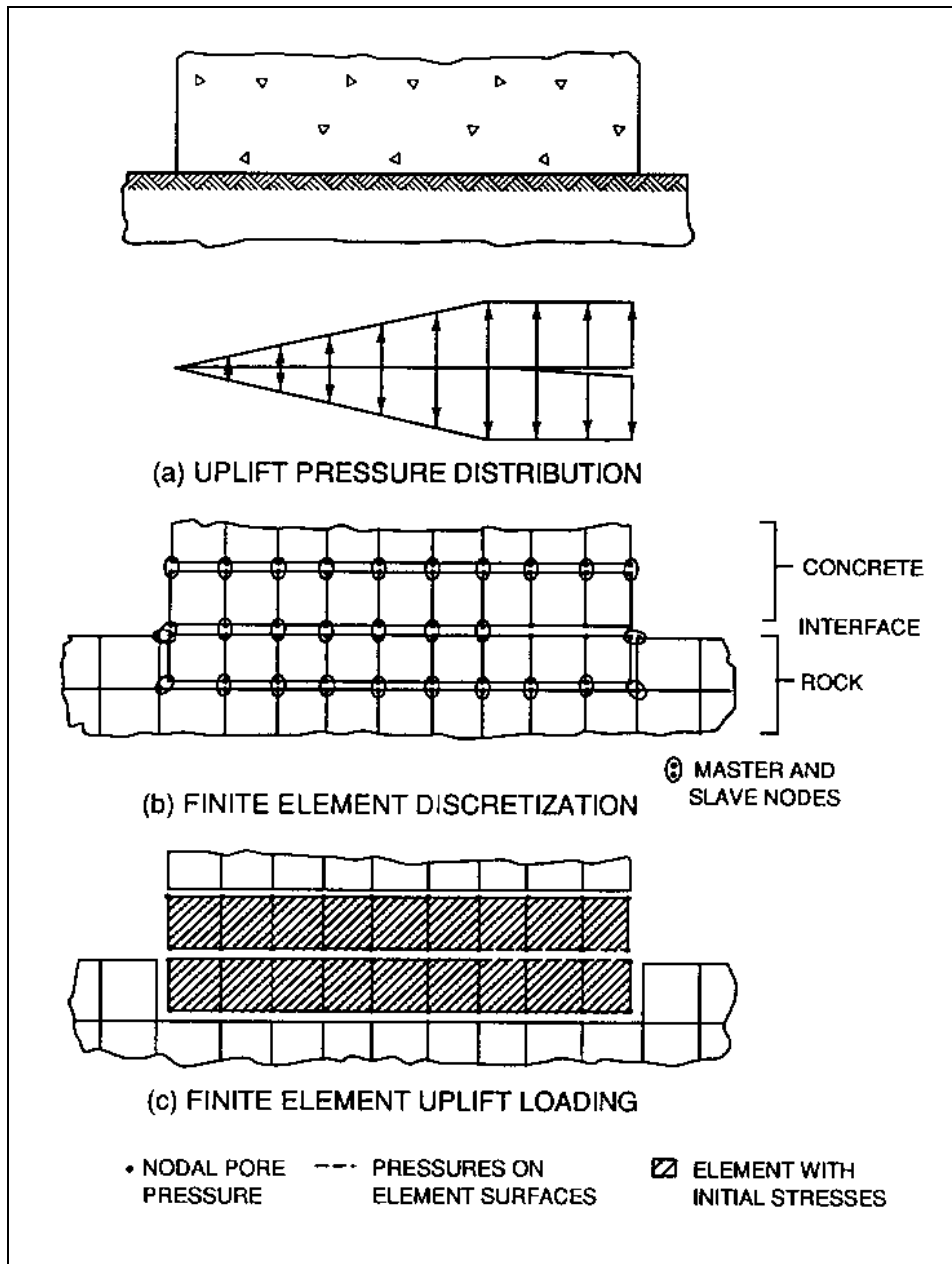


Figure A-7. Modeling of uplift pressures

stresses resulting from pore pressures are isolated from the rest of the mesh by master and slave nodes. This allows for a discontinuity in the normal stresses on shared element boundaries for elements with and without initial stresses. The stresses computed in the elements subject to initial stresses  $\sigma_0$  are the effective stresses  $\sigma'$ ; total stresses  $\sigma$  are obtained by adding the initial and effective stresses

$$\sigma = \sigma' + \sigma_0 \quad (8)$$

In the absence of pore pressures, the effective and total stresses are identical.

(c) Computation of stress intensity factors. Stress intensity factors ( $K_I$  for opening mode I, and

$K_{II}$  for shearing mode II; see ETL 1110-8-16(FR) Figure 1-2) are computed using a contour integral method based on a reciprocal work theorem (Stern, Becker, and Dunham 1976). The method is modified to include the contributions of body forces, initial stresses, and pressures on the crack surfaces. Comparisons between the modified contour integral method and the displacement correlation method have shown that the computed stress intensity factors are within engineering accuracy (ETL 1110-8-16(FR)). When initial stresses due to pore pressures are present, the effective stresses are used to compute the contour integral. Since the deformations and stresses in the foundation due to self weight occurred before the lock was constructed, the corresponding body forces in the foundation do not contribute to the computed stress intensity factors. Assigning a value of zero to the unit weight of the rock eliminates body forces in the foundation and no special logic is required to eliminate their contribution from the computed stress intensity factors.

*d. Analysis and results.*

(1) Estimation of crack length.

(a) For the method of analysis used in this study, the estimation of crack length for a crack at the base of the monolith requires an iterative approach. The basic approach involves running several analyses each with a different crack length, with the goal of obtaining a calculated value of  $K_I = K_{Ic}$ . For each analysis, the value of  $K_I$  is computed and compared to  $K_{Ic}$ . If  $K_I$  is larger than  $K_{Ic}$ , this indicates that the crack will propagate under the given conditions and a subsequent analysis with a longer specified crack length is performed. If  $K_I$  is less than  $K_{Ic}$ , the crack will not propagate and a subsequent analysis with a shorter crack length is performed. For all analyses performed in this study, it was assumed that  $K_{Ic} = 0.0 \text{ ksi}\sqrt{\text{in.}}$ . The structural analysis is therefore reduced to a finite element analysis with fracture mechanics used as the criterion for crack extension.

(b) A series of six analyses, each with a different specified crack length, was performed using the MERLIN computer program (Reich, Cervenka, and Saouma 1991) to obtain an initial estimate of the crack length. The crack lengths for these analyses ranged from 6.0 to 13.5 ft in 1.5-ft increments,

which was chosen based on the element size (i.e., those adjacent to the monolith/foundation). No analyses were performed for crack lengths greater than 13.5 ft because the computed value of  $K_I$  for a crack length of 13.5 ft was negative and  $K_I$  was positive for all prior analyses. A final crack length of 12.99 ft was estimated by interpolation of results of  $K_I$  for analyses with crack lengths between 12 ft and 13.5 ft (based on a value of zero for  $K_{Ic}$ .)

(c) Additional analyses were performed to determine a more precise value for the final crack length. In these analyses, re-meshing was performed by relocating a pair of nodes on the interface between the monolith and the foundation to the estimated position of the crack tip. To accommodate uplift forces, node pairs on the boundaries between elements with and without initial stresses that were originally directly above or below the crack tip nodes are repositioned in the horizontal direction along with the crack tip nodes to keep all elements rectangular. The modified mesh was reanalyzed to determine the corresponding stress intensity factors. This procedure was repeated until the value of  $K_I$  was less than  $0.001 \text{ ksi}\sqrt{\text{in.}}$  ( $0.0011 \text{ MPa}\sqrt{\text{m}}$ ). The final crack length computed using this approach was 13.02 ft, which is 43.7% less than the 23.13 ft predicted by the traditional method of analysis. The results of the first six analyses and the analysis yielding the final crack length are summarized in Table A-2. For each crack length  $a$ , the stress intensity factors for modes I ( $K_I$ ) and II ( $K_{II}$ ), crack mouth opening displacement (CMOD), and the horizontal crest displacement  $\Delta H_{\text{crest}}$  are given. Negative values for the horizontal crest displacements indicate movement into the lock chamber.

(2) Variation of stress intensity factors. The variations in  $K_I$  and  $K_{II}$  as a function of crack length are shown in Figure A-8. The value of  $K_I$  decreases with increasing crack length and equals zero at a crack length of 13.02 ft. Since the fracture toughness is assumed to be zero, the final estimated crack length corresponds to this crack length. If a less conservative value had been assumed for the fracture toughness, the final predicted crack length would have been shorter. For example, a realistic value of  $K_{Ic}$  for concrete is approximately  $1.0 \text{ ksi}\sqrt{\text{in.}}$  and the resulting predicted crack length for  $K_{Ic} = 1.0 \text{ ksi}\sqrt{\text{in.}}$  would be less than 6.0 ft. Because  $K_I$  decreases as the crack length is increased, this particular combination of

**Table A-2**  
**Summary of Finite Element Analyses**

$a$ ft	$K_I$ ksi $\sqrt{\text{in.}}$	$K_{II}$ ksi $\sqrt{\text{in.}}$	CMOD in.	$\Delta H_{\text{crest}}$ in.
6.00	0.868	0.489	0.0111	-0.0806
7.50	0.743	0.483	0.0127	-0.0847
9.00	0.581	0.492	0.0140	-0.0881
10.50	0.387	0.521	0.0150	-0.0908
12.00	0.162	0.582	0.0155	-0.0924
13.02	0.000	0.643	0.0154	-0.0925
13.50	-0.083	0.678	0.0153	-0.0924

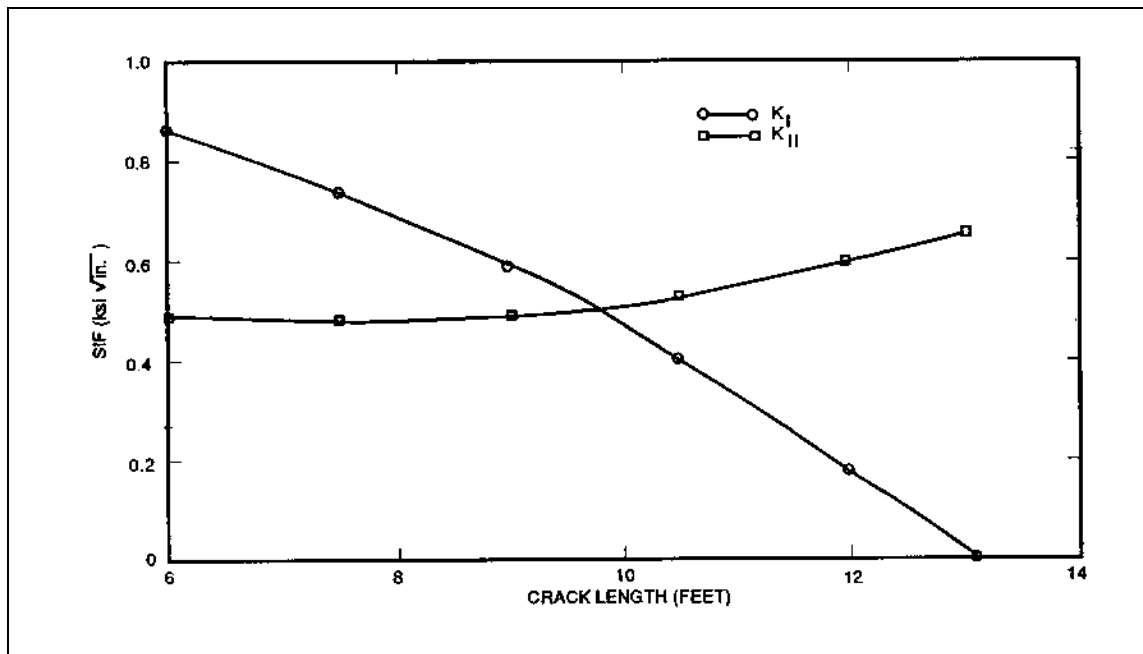


**Figure A-8.  $K_I$  and  $K_{II}$  versus crack length for the monolith**

geometry and loading constitutes a stable fracture geometry. An increase in  $K_I$  as the crack length is increased would constitute an unstable fracture geometry. For a stable fracture geometry in equilibrium, the loading must be increased in order for the crack to propagate and propagation will cease when a new equilibrium configuration is reached. An unstable fracture geometry leads to a catastrophic failure unless the loading somehow changes to create a stable fracture geometry once a crack begins to propagate. Because this is a stable fracture geometry, the horizontal and vertical uplift forces acting to open the crack and the vertical forces acting to close the crack reach an equilibrium configuration, and crack propagation ceases. For

these analyses,  $K_I$  decreases with increasing crack length because the gravity forces acting to close crack become more dominant. Figure A-8 shows that the value of  $K_{II}$  is relatively constant for crack lengths between 6.0 and 9.0 ft, but increases with crack length beyond 9.0 ft. If  $K_{II}$  is of sufficient magnitude, the crack direction may change. When significant shear stress (related to  $K_{II}$ ) is combined with the normal stress, the direction of maximum tension stress changes. For a competent material (homogeneous and defect free), the direction of the crack will propagate perpendicular to the direction of greatest tension. For materials that are not homogeneous and defect free, the crack will propagate where a much lower  $K_{Ic}$  value exists or where

there is a nearby pre-existing crack. For the Locks 27 monolith, data on the exact condition of the interface bond and foundation does not exist. If it is assumed that the interface bond is perfect and the monolith and foundation materials are homogeneous and defect free, the crack may curve away from the interface, as the crack length increases beyond 9.0 ft.

(3) Crack opening displacement profiles. The crack opening displacement (COD) profiles for assumed crack lengths of 6.0 to 13.02 ft are shown in Figure A-9. The COD profiles for crack lengths of 6.0 through 10.5 ft exhibit noticeable kinks near the crack tip which are not evident for longer crack lengths. This effect is a function of the coarseness of the mesh. As described, these results represent cases where  $K_{Ic} = K_I$  of Table A-2. For shorter crack lengths  $K_{Ic}$  would be larger; therefore, higher tensile stresses can develop at the uncracked region near the crack tip causing higher displacement gradients. The mesh is too coarse to capture the high displacement gradients evident for shorter crack lengths; therefore, some distortion of the plotted displacements occurs in the region near the crack tip. As the crack length increases, the displacement gradients near the crack tip decrease (due

to lower  $K_{Ic}$ ) and the mesh is better able to capture them.

(4) Normal stress profiles.

(a) The normal stress (effective stress) profiles along the base of the monolith for crack lengths of 6.0 to 13.02 ft are shown in Figure A-10. The normal stress profiles are virtually identical for distances along the base of the monolith up to 25.0 ft. Beyond 25.0 ft, the normal stress profiles diverge. This lack of sensitivity to the crack length in the normal stresses at less than 25.0 ft is the result of the relatively large culvert in close proximity to the interface between the monolith and the foundation. There is only 8.0 ft between the bottom of the culvert and the top of the foundation and the width of the culvert is almost one third that of the entire monolith. The portion of the monolith under the culvert lacks sufficient stiffness to transfer vertical stresses, effectively isolating the right side of the monolith from the left side near the base. In order to further determine the effect of the culvert, an additional series of analyses was performed in which the culvert was not considered. The results of these analyses are summarized in Appendix B.

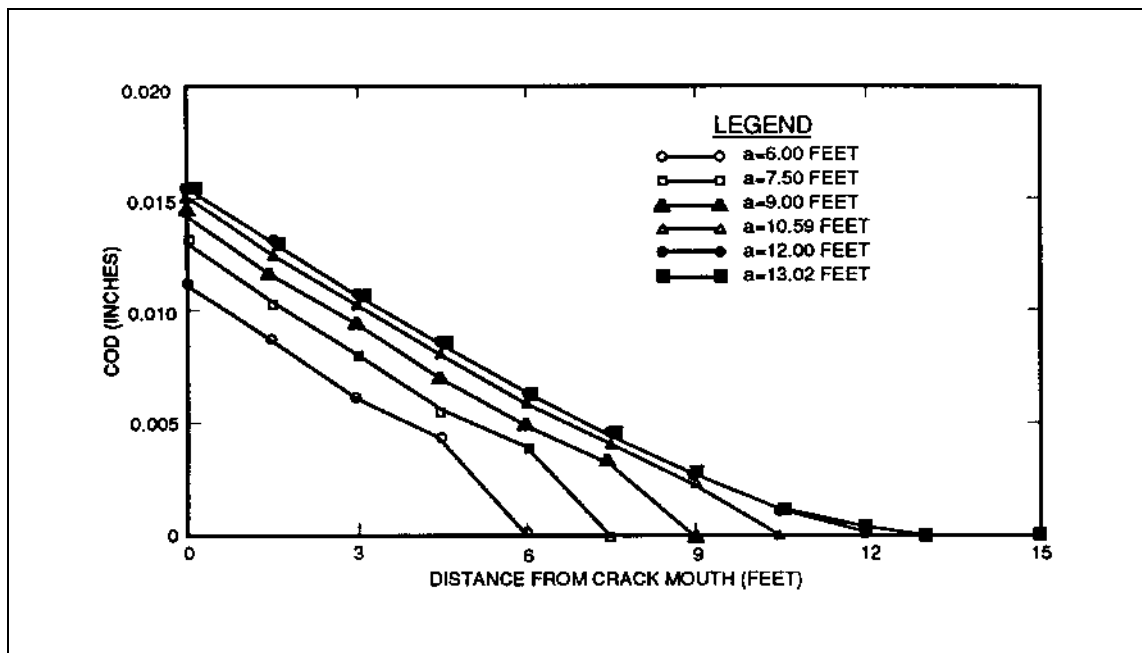


Figure A-9. COD profiles for cracks at the base of monolith

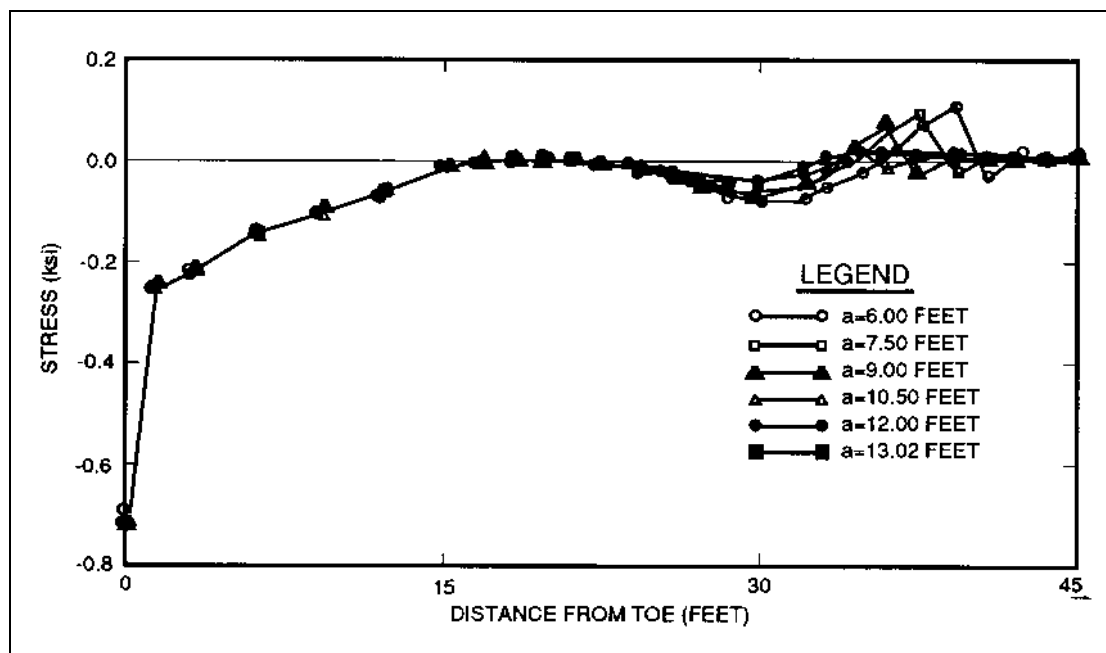


Figure A-10. Normal stress profiles at the base of the monolith

(b) The normal stress profiles along the base of the monolith for the final crack lengths predicted by both the finite element analysis and the traditional method of analysis are shown in Figure A-11. The effective stress is plotted as a function of distance along the base of the monolith (with the toe located at zero) and the negative sign on the stresses indicates compression. The stress computed from the finite element analysis was integrated along the base using the Trapezoidal rule to determine the resultant force in the vertical direction. In order to assess the accuracy of the finite element analysis, the resultant force was also computed for a crack length of 13.02 ft using the assumed stress distribution of the traditional analysis technique. The crack length of 13.02 ft was used in this computation rather than the predicted crack length of 23.13 ft because the uplift forces are a function of the crack length and any other crack length would result in nonequivalent force systems. A crack length of 13.02 ft yields a tensile stress at the crack tip using the traditional analysis technique. The tensile stresses were included in calculation of resultant forces because this comparison is between two equivalent force systems, not systems with equivalent crack lengths. The resultant force from the finite element analysis was 416.64 kips/ft (kips per foot width) as opposed to 414.37 kips/ft from the traditional analysis technique. Similar computations were also

performed to determine the line of action for the resultant forces from the two methods of analysis. The line of action for the resultant force from the finite element analysis was 7.60 ft to the right of the toe as opposed to 7.29 ft from the traditional analysis technique. Confidence in the finite element analysis is provided since the results show a good correlation between the two methods of analysis.

(5) Shear stress profiles. The shear stress profile along the base of the monolith for a crack length of 13.02 ft is shown in Figure A-12. The integrated stress was computed to determine the resultant force in the horizontal direction resulting in a value of 247.82 kips. Comparison to 249.78 kips from the traditional method of analysis shows a good correlation.

(6) Vertical displacement profiles. The vertical displacement profiles along the base of the monolith for crack lengths of 6.0 to 13.02 ft are shown in Figure A-13. The vertical displacement profiles are virtually identical for distances along the base of the monolith up to 20.0 ft. Beyond 20.0 ft, the vertical displacement profiles diverge. The explanation for this phenomenon follows the same line of reasoning as that for the behavior of the normal stresses along the base of the monolith, in which the culvert near the interface between

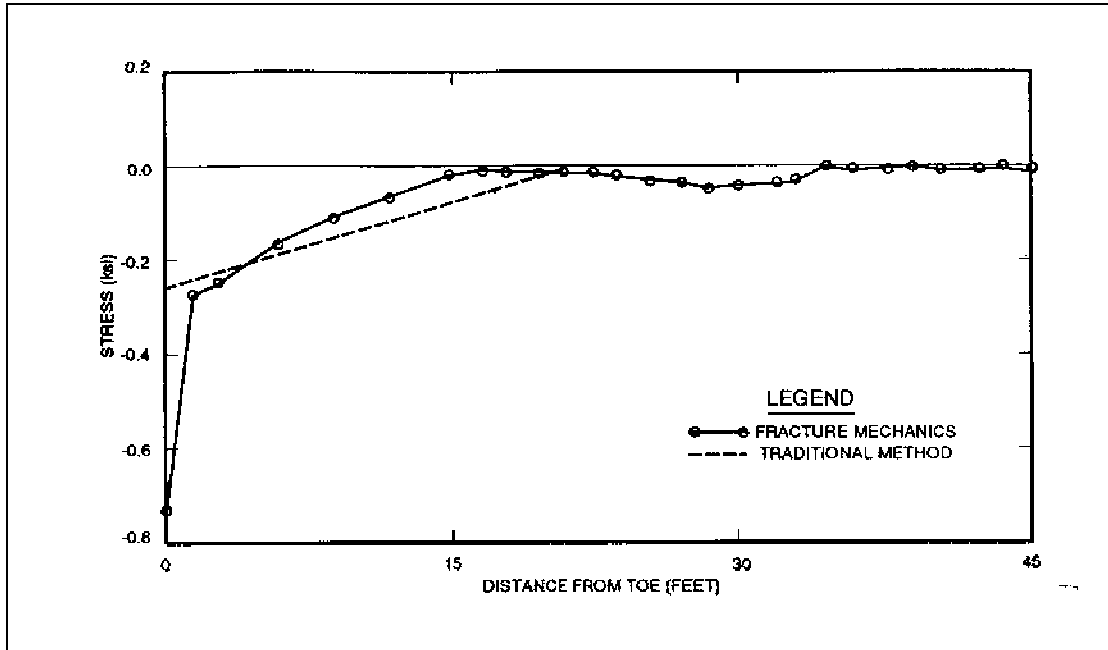


Figure A-11. Normal stress profile at the base of monolith for  $a = 13.02$  ft

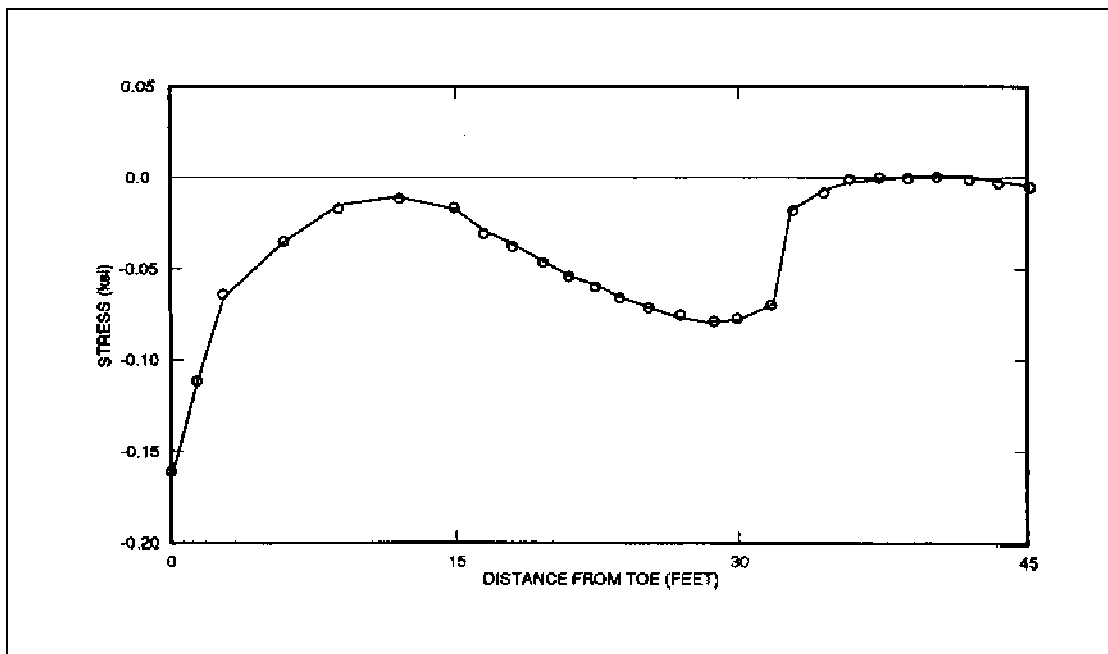


Figure A-12. Shear stress profile at the base of monolith for  $a = 13.02$  ft

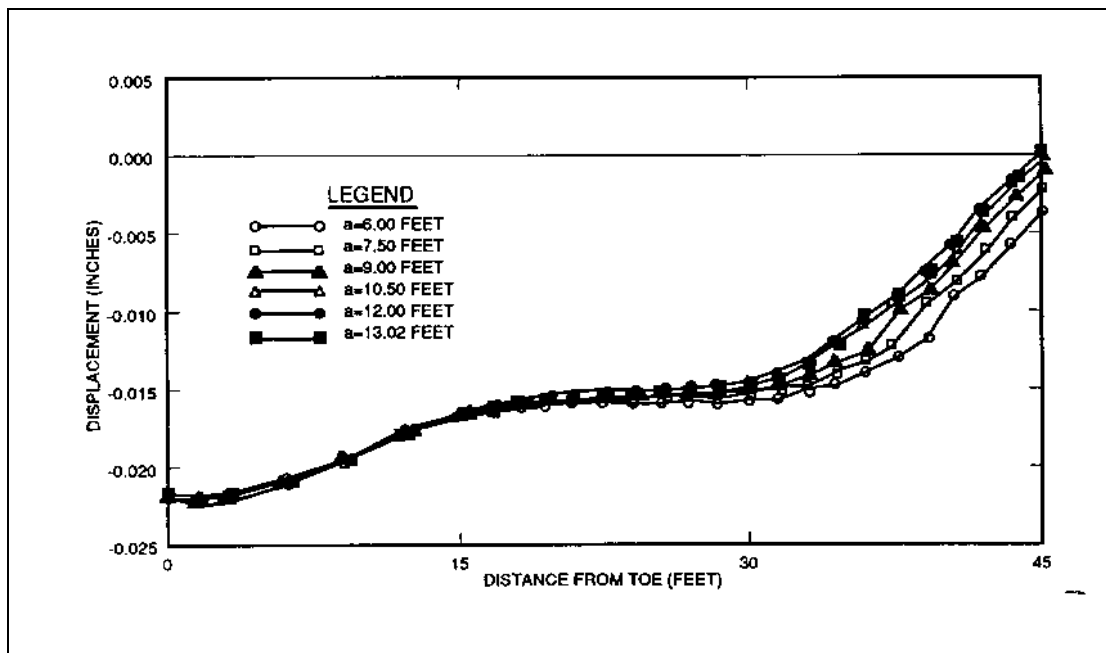


Figure A-13. Vertical displacement profiles at the base of monolith

the monolith and the foundation directly influences the results on the interface.

#### 4. Comparison of Current Practice and Fracture Mechanics Analyses

The crack length computed from the finite element fracture mechanics based analyses assuming a fracture toughness of zero ( $K_{Ic} = 0$ ) is 13.02 ft. The percentage of base in compression for a crack length of 13.02 ft is 71%, which is near, yet still does not satisfy the 75% criteria required by ETL 1110-2-22. The crack length computed by the traditional method of analysis was 23.13 ft, which yields a percentage of base in compression of 48.6%.

#### 5. Conclusion

*a. Mode II consideration.* The computed values for  $K_{II}$  are relatively large, even for shorter crack lengths. As the crack length increases,  $K_{II}$  is the dominant stress intensity factor because while the value  $K_I$  decreases with crack length the value of  $K_{II}$  increases. This trend indicates that the preferred path of the crack would be curved, provided the bond at the interface is good and the foundation

material is competent. For the Locks 27 monolith, data on the exact condition of the interface bond and foundation does not exist. If it is assumed that the interface bond is perfect and the monolith and foundation materials are homogeneous and defect free, confining the crack to the interface may not be realistic. For longer crack lengths, the tendency for the crack to deviate from the interface becomes more pronounced.

*b. Analysis consideration.* The traditional method of analysis appears to be overly conservative in comparison to the finite element fracture mechanics based method of analysis for this particular monolith geometry and the applied load conditions. This observation was partially confirmed by field measurements when the lock was dewatered and should be accounted for. As opposed to the traditional method of analysis, the proposed method of analysis is more realistic for two reasons. First, the deformation of the monolith and foundation are considered through elastic analysis, and secondly, the behavior at a crack tip is more realistically characterized by fracture mechanics. When expensive rehabilitation procedures are being considered solely on the basis of the traditional method of analysis, a fracture mechanics based solution may yield a less expensive rehabilitation program without jeopardizing structural safety.

## APPENDIX B: ANALYSES WITH NO CULVERT

### 1. Introduction

In an effort to determine the effects of the large culvert located near the base of the monolith, a series of analyses was performed for a solid monolith in which the culvert was not considered. Analysis procedures were identical to those described in Appendix A. The open area of the culvert was eliminated by simply adding elements and nodes to the mesh shown in Figure A-4 of Appendix A. Material properties and applied loads for this investigation were identical to those used for the analyses in which the culvert was considered.

### 2. Analysis and Results

#### a. Estimation of crack length.

(1) A series of nine analyses, each with a different specified crack length, was performed to compute an initial estimate of the final crack length. The prescribed crack lengths for these analyses ranged from 6.0 ft to 18.0 ft in 1.5-ft increments. No analyses were performed for crack lengths greater than 18.0 ft because the value of  $K_I$  for  $a = 18$  ft was negative and  $K_I$  was positive for all prior analyses. The final crack length of 16.65 ft was found by re-meshing and comparing  $K_I$  to  $K_{Ic}$  as described in paragraph 3d(1) of Appendix A. The results of each analysis are summarized in Table B-1. The variations of  $K_I$  and  $K_{II}$  over the range of crack lengths are shown in Figure B-1.

(2) The final crack length computed using the traditional method of analysis was 19.62 ft. The fracture mechanics based prediction of 16.65 ft is only 15.1% less than the value of 19.62 ft computed using the traditional analysis method. When the culvert was considered, the discrepancy between the final crack lengths was 43.7% (see Appendix A), which is slightly more than three times the 15.1% of this case. The fact that the estimated crack lengths are in much better agreement when the culvert is not considered indicates that the rigid behavior assumed by the traditional method of analysis more closely approximates the actual behavior as the monolith becomes stiffer. This should be expected since a solid monolith would behave more like a rigid block than one with a large culvert. Based on this observation, the assumption of a rigid monolith in the traditional method of analysis does not appear to be valid when a large culvert is present.

#### b. Normal stress profiles.

(1) The normal stress profile along the base of the monolith for a crack length of 16.65 ft is shown in Figure B-2. In order to contrast the difference between the traditional and proposed methods of analysis, the normal stress profile from the traditional method of analysis is also included in Figure B-2. The distance along the base of the monolith is measured from the toe of the monolith to the heel of the monolith and a negative stress indicates compression. Comparison of the normal

**Table B-1**  
**Summary of Finite Element Analyses With No Culvert**

$a$ ft	$K_I$ ksi $\sqrt{\text{in.}}$	$K_{II}$ ksi $\sqrt{\text{in.}}$	CMOD in.	$\Delta H_{\text{crest}}$ in.
6.00	0.566	0.628	0.00715	-0.0667
7.50	0.500	0.648	0.00791	-0.0690
9.00	0.435	0.665	0.00859	-0.0712
10.50	0.366	0.682	0.00919	-0.0732
12.00	0.291	0.700	0.00969	-0.0750
13.50	0.209	0.719	0.01006	-0.0764
15.00	0.117	0.740	0.01028	-0.0775
16.50	0.012	0.764	0.01028	-0.0780
16.65	0.000	0.766	0.01027	-0.0770
18.00	-0.108	0.792	0.00962	-0.0748

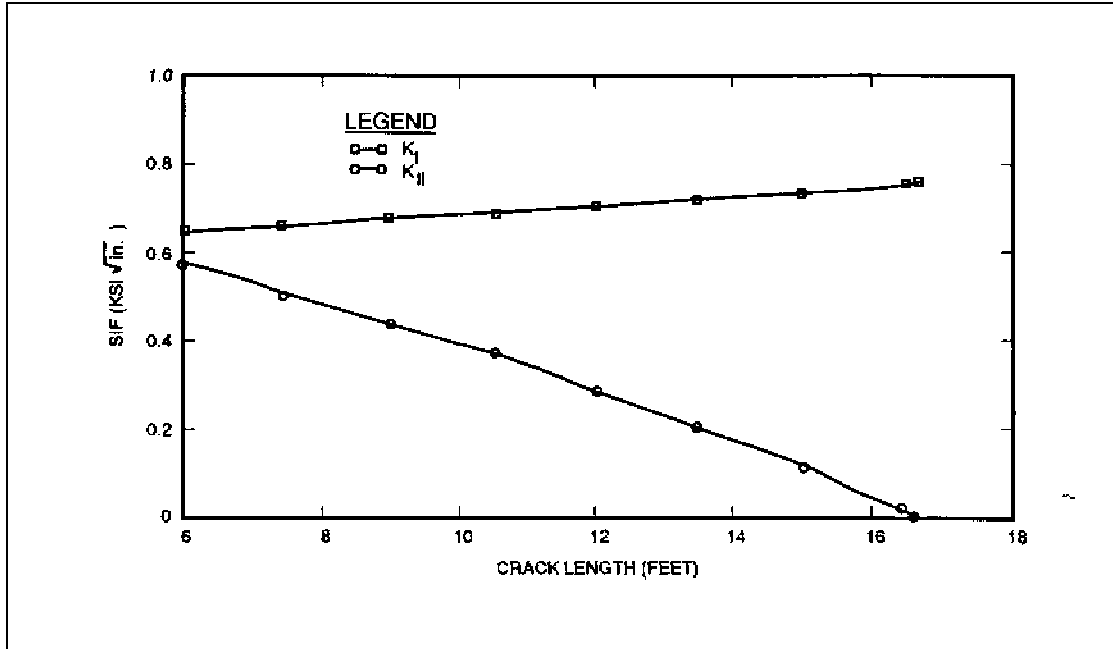


Figure B-1.  $K_I$  and  $K_{II}$  versus crack length for monolith: no culvert

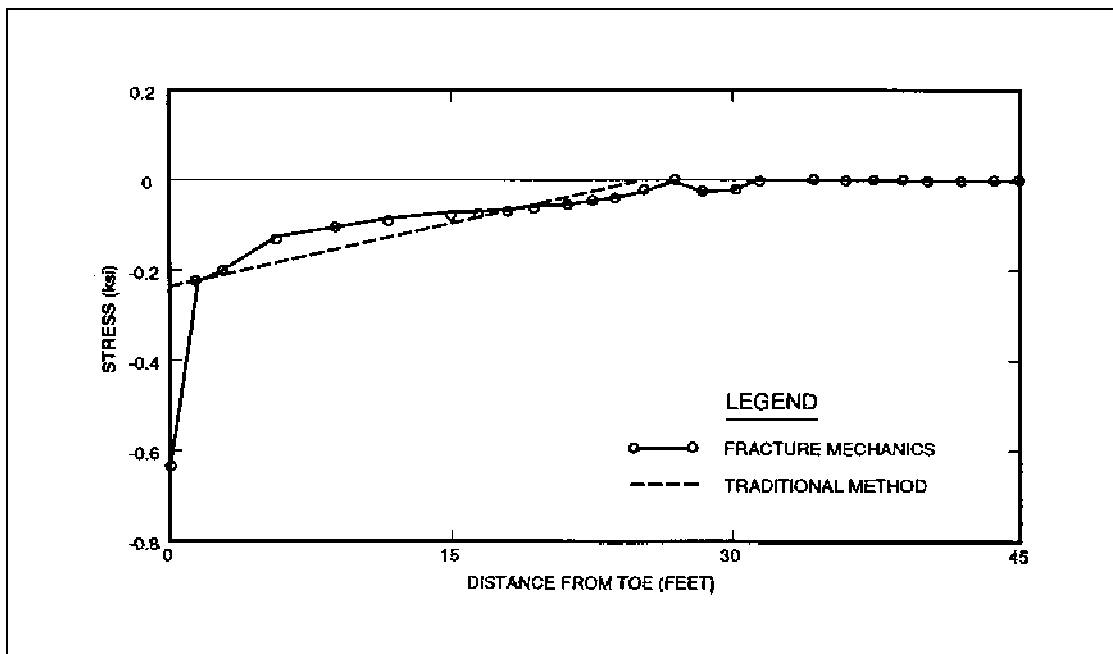


Figure B-2. Normal stress profile at the base of monolith for  $a = 16.65$  ft: no culvert

stress profiles of the no-culvert case (Figure B-2) and the actual case (Figure A-11 of Appendix A) shows the effect of the culvert on the normal stress profile. The variation of normal stresses to near zero values between 15.0 and 25.0 ft in Figure A-11 of Appendix A does not exist in the stress profile of Figure B-2. The normal stress profile of Figure B-2 exhibits a near linear response from a location near the monolith toe to the crack tip. This response is more closely approximated using the traditional method of analysis. This provides further validity to the argument that the proximity of the culvert to the base of the monolith has a substantial effect on the transfer of normal stresses in that region.

(2) The resultant force in the vertical direction and the line of action for the resultant force were computed for the finite element solution (as described in paragraph 3d(4) of Appendix A) and for the traditional analysis technique. An equivalent force system with a crack length of 16.65 ft rather than the final crack length of 19.62 ft was used in the computations using assumptions of the traditional analysis technique. The calculated resultant force for the finite element analysis was 447.97 kips

as opposed to 440.56 kips for the traditional analysis technique. The line of action for the resultant force from the finite element analysis was 8.58 ft to the right of the toe as opposed to 8.57 ft from the traditional analysis technique.

*c. Shear stress profile.* The shear stress profile along the base of the monolith for a crack length of 16.65 ft is shown in Figure B-3. The distance along the base of the monolith is measured from the toe of the monolith to the heel of the monolith. The effect of the culvert is shown further by comparison of results of the no culvert case (Figure B-3) and the case considering the culvert (Figure A-12 of Appendix A). The shear stress profile of Figure B-3 is relatively constant except for the edge effects. However, the variation in shear stresses of Figure A-12 of Appendix A is more significant. The resultant horizontal force was computed for the finite element solution by integration of the stress along the base of the monolith and the traditional analysis technique. The resultant force from the finite element analysis was 247.45 kips as opposed to 249.78 kips from the traditional analysis technique.

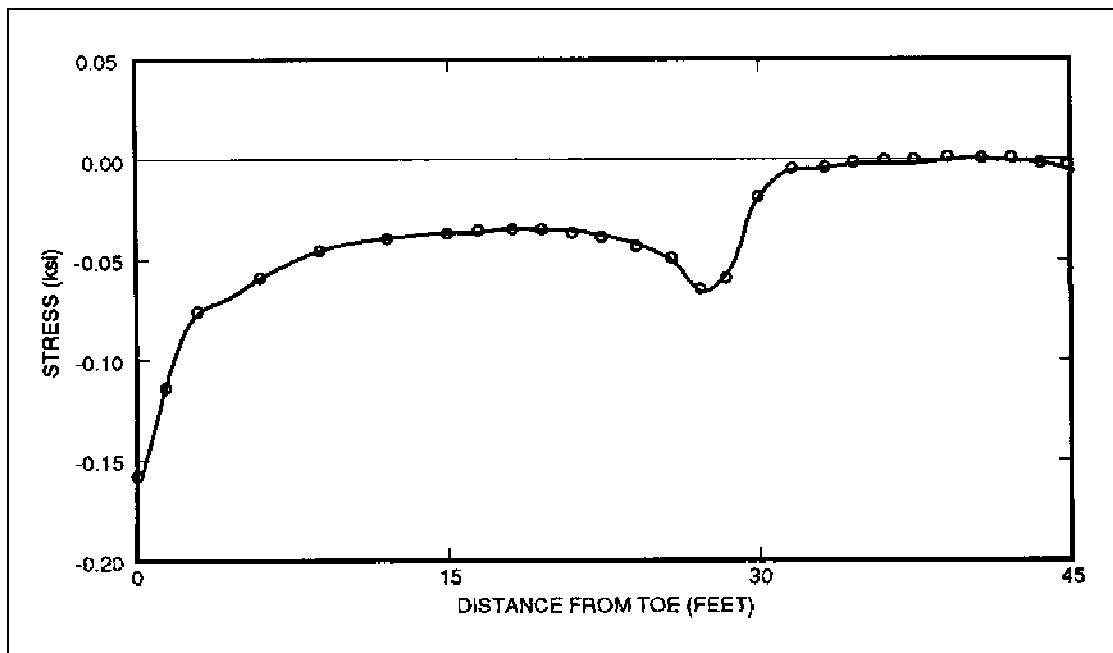


Figure B-3. Shear stress profile at the base of monolith for  $a = 16.65$  ft: no culvert

## APPENDIX C: ANALYSES WITH NO UPLIFT

### 1. Introduction

In an effort to simplify the comparison between the traditional method of analysis and the finite element/fracture mechanics based analysis, a series of analyses was performed for monolith 7E in which the uplift pressure at the base of the monolith was not considered (the culvert was considered in this case). Neglecting the uplift pressure greatly simplifies both the modeling of the structure and the computation of the stress intensity factors. The master and slave nodes required to model that portion where the uplift pressure was applied as pore pressures (initial stresses) were not present in the mesh used for these analyses. Otherwise the mesh was identical to the one shown in Figure A-4 of Appendix A. The material properties and the remaining applied loads for this investigation were not changed from those used for the analyses described in Appendix A in which uplift was considered.

### 2. Analysis and Results

#### a. Estimation of crack length.

(1) A series of three analyses, each with a different specified crack length, was performed to compute an initial estimate of the final crack length. The prescribed crack lengths for these analyses ranged from 6.0 ft to 9.0 ft in 1.5-ft increments. No analyses were performed for crack lengths greater than 9.0 ft because the value of  $K_I$  was negative for a crack length of 9.0 ft and  $K_I$  was positive for all prior analyses. The final crack length of 8.58 ft was found by re-meshing and comparing  $K_I$  to  $K_{Ic}$  as described in paragraph 3d(1) of Appendix A. However, since initial stresses were not prescribed for elements adjacent to the interface between the

monolith and the foundation, it was required only to reposition the pair of nodes on the monolith/foundation interface. The results of these analyses are summarized in Table C-1. The variations of  $K_I$  and  $K_{II}$  over the range of crack lengths are shown in Figure C-1.

(2) The final crack length computed using the traditional method of analysis was 9.55 ft. The value of 8.58 ft computed using finite element analysis and fracture mechanics is only 10.2% less than 9.55 ft. When uplift was considered, the discrepancy between the final crack lengths was 43.7% (see Appendix A), which is over four times the 10.2% predicted for this case. The improved agreement in the predicted final crack lengths may be an indication that the crack length of 8.58 ft is not long enough to be strongly influenced by the culvert. Even though the culvert is relatively large in relation to the monolith, the influence that it would have on the stresses and displacements at the base of the monolith is greatest near the culvert and decreases as the distance from the culvert increases. Based on the observed results, the discrepancy between the two methods of analysis would be even less if both the culvert and the uplift were not considered.

#### b. Normal stress profiles.

(1) The normal stress profile along the base of the monolith with a crack length of 8.58 ft and no uplift is shown in Figure C-2. In order to contrast the difference between the traditional and proposed methods of analysis, the normal stress profile from the traditional method of analysis is also included in Figure C-2. In comparing Figure C-2 (no uplift case) with Figure A-11 of Appendix A (full uplift case) the effect of the uplift on the normal stress profile is minor considering the overall shape of the

**Table C-1**  
**Summary of Finite Element Analyses With No Uplift**

a ft	$K_I$ ksi $\sqrt{\text{in.}}$	$K_{II}$ ksi $\sqrt{\text{in.}}$	CMOD in.	$\Delta H_{\text{crest}}$ in.
6.00	0.411	0.536	0.00800	-0.0762
7.50	0.188	0.536	0.00843	-0.0777
8.58	0.000	0.547	0.00842	-0.0781
9.00	-0.132	0.578	0.00835	-0.0781

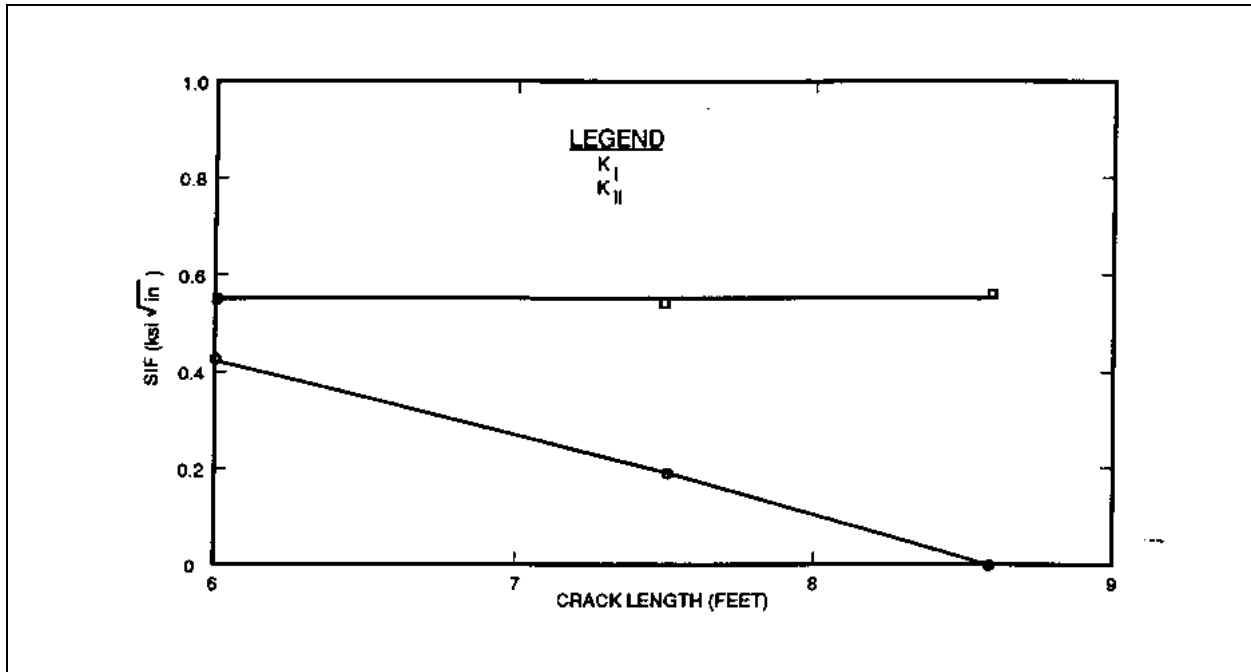


Figure C-1.  $K_I$  and  $K_{II}$  versus crack length for monolith: no uplift

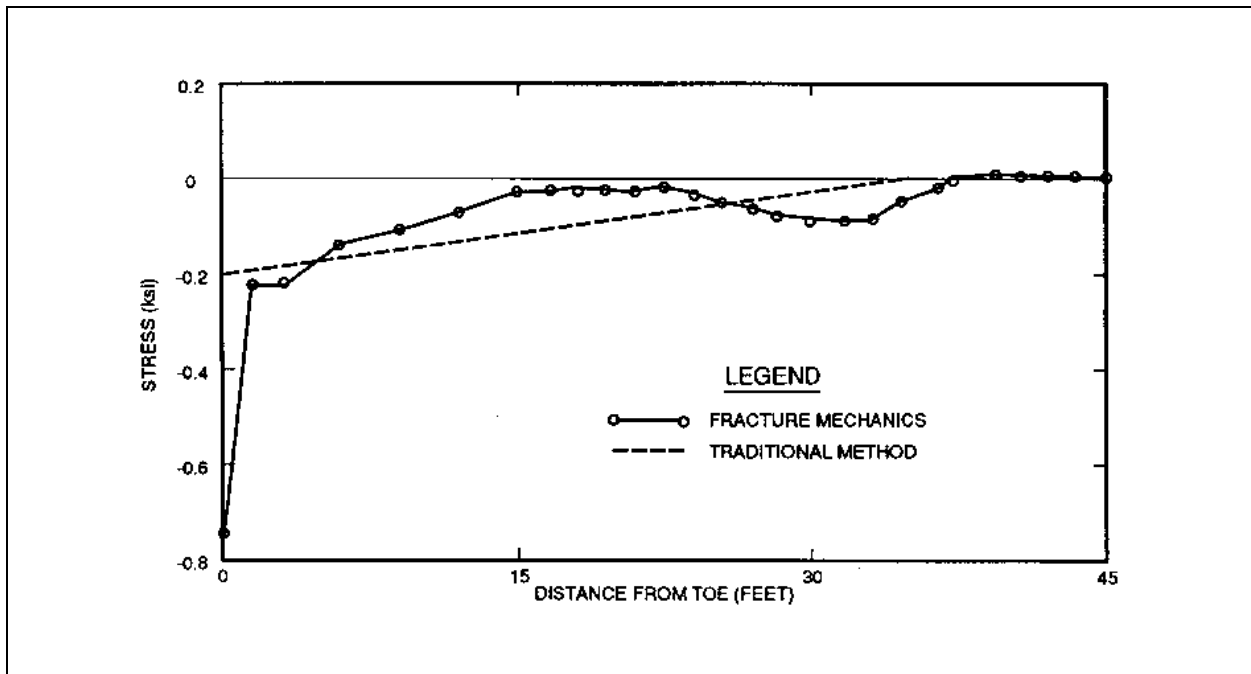


Figure C-2. Normal stress profile at the base of monolith for  $a = 8.58$  ft: no uplift.

curves. In all plots showing normal stress profiles (Figures A-11 of Appendix A, B-2 of Appendix B, and C-2), the normal stress near the crack tip is a relatively small negative value instead of zero. These errors in the normal stress are a consequence of the nodal strain projection technique, which is very sensitive to the level of mesh refinement around sharp corners and notches. However, the normal stresses on the crack surface at a short distance away from the crack tip are zero in all cases. This demonstrates that the effect of the crack tip on the nodal stresses is indeed local and that the small error in the normal stress at the crack tip should not be a cause for concern.

(2) The resultant force in the vertical direction and the line of action for the resultant force were computed for the finite element solution and the traditional analysis technique. Since uplift was not considered, the actual estimated final crack lengths for the two methods of analysis were used in these computations (with no uplift, the two systems are equivalent force systems regardless of crack length). The calculated resultant force from the finite element analysis was 519.41 kips as opposed to 515.90 kips from the traditional analysis technique.

The line of action for the resultant force from the finite element analysis was 11.79 ft to the right of the toe as opposed to 11.82 ft from the traditional analysis technique.

*c. Shear stress profiles.* The shear stress profile along the base of the monolith for a crack length of 8.58 ft is shown in Figure C-3. In comparing Figure C-3 with Figure A-12 of Appendix A the effect of the uplift on the shear stress profile is minor in terms of the overall shape of the curves, as was the case with the normal stresses. However, the shear stress profile in Figure C-3 does show a slight increase between the right side of the culvert and the crack tip before going to zero on the crack surface. It could be argued that this demonstrates that the effect of the culvert on stresses (and displacements) at the base of the monolith may be limited to certain cases. The resultant force in the horizontal direction was computed for the finite element solution and the traditional analysis technique. The resultant force from the finite element analysis was 250.62 kips as opposed to 249.78 kips from the traditional analysis technique.

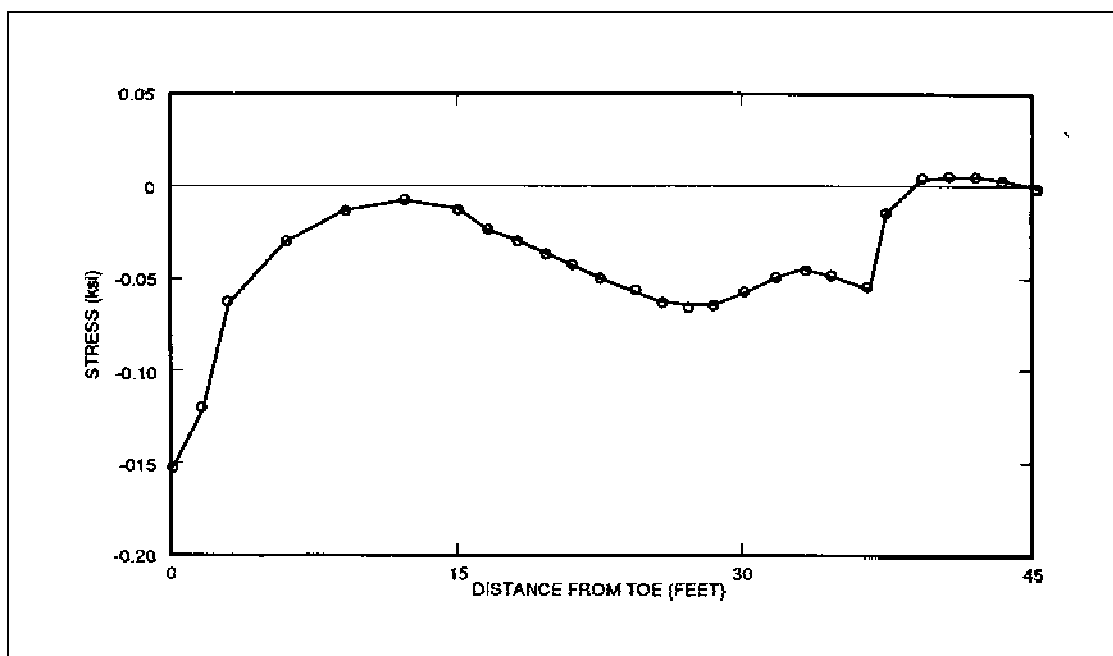


Figure C-3. Shear stress profile at the base of monolith for  $a = 8.58$  ft: no uplift